

Talk2Radar: Bridging Natural Language with 4D mmWave Radar for 3D Referring Expression Comprehension

Runwei Guan^{1,2,5}*, Ruixiao Zhang³*, Ningwei Ouyang^{1,2,5}*, Jianan Liu⁴*, Ka Lok Man⁵, Xiaohao Cai³, Ming Xu^{2,5}, Jeremy Smith², Eng Gee Lim⁵, *Senior Member, IEEE*, Yutao Yue^{6,7,1}†, Hui Xiong⁶, *Fellow, IEEE*

Abstract—Embodied perception is essential for intelligent vehicles and robots, enabling more natural interaction and task execution. However, these advancements currently embrace vision level, rarely focusing on using 3D modeling sensors, which limits the full understanding of surrounding objects with multi-granular characteristics. Recently, as a promising automotive sensor with affordable cost, 4D Millimeter-Wave radar provides denser point clouds than conventional radar and perceives both semantic and physical characteristics of objects, thus enhancing the reliability of perception system. To foster the development of natural language-driven context understanding in radar scenes for 3D grounding, we construct the first dataset, Talk2Radar, which bridges these two modalities for 3D Referring Expression Comprehension. Talk2Radar contains 8,682 referring prompt samples with 20,558 referred objects. Moreover, we propose a novel model, T-RadarNet for 3D REC upon point clouds, achieving state-of-the-art performances on Talk2Radar dataset compared with counterparts, where Deformable-FPN and Gated Graph Fusion are meticulously designed for efficient point cloud feature modeling and cross-modal fusion between radar and text features, respectively. Further, comprehensive experiments are conducted to give a deep insight into radar-based 3D REC. We release our project at <https://github.com/GuanRunwei/Talk2Radar>.

Index Terms—3D referring expression comprehension, 3D visual grounding, 4D mmWave radar, multi-modal fusion

I. INTRODUCTION

Millimeter-wave (mmWave) radar, as an all-weather and low-cost perception sensor [1, 2] which can capture objects’ distance, azimuth, velocity, motion directions, reflected power, etc, has been commonly used in perception for autonomous driving [3–8], robotic navigation [9, 10] and Cooperative Intelligent Transportation Systems (C-ITS) [11]. Recently, to enhance the detection accuracy, 4D radar appears and addresses the limitation of conventional radar’s inability to measure height and significantly increases Point Cloud (PC) density [12, 13]. This allows captured objects to contain more exploitable features for more fruitful scene understanding and better performance in different downstream tasks on land [14–19] and maritime [20–22].

This work has been submitted to the IEEE for possible publication. Copyright may be transferred without notice, after which this version may no longer be accessible.

* R. Guan, R. Zhang, N. Ouyang and J. Liu contribute equally.

¹ Institute of Deep Perception Technology, JITRI, Wuxi, China

² Department of EEE, University of Liverpool, Liverpool, UK

³ School of ECS, University of Southampton, Southampton, UK

⁴ Vitalent Consulting, Gothenburg, Sweden

⁵ SAT, Xi’an Jiaotong-Liverpool University, Suzhou, China

⁶ Thrust of Artificial Intelligence, HKUST (GZ), Guangzhou, China

⁷ Thrust of Intelligent Transportation, HKUST (GZ), Guangzhou, China

† Corresponding author: yutaoyue@hkust-gz.edu.cn

Meanwhile, with recent advancements driven by Vision-Language Models (VLMs) [23] in embodied intelligence and human-centric intelligent driving perception systems [24], VLMs and Multi-Modal Large-Language Models (MM-LLMs) enable intelligent vehicles and robots to understand human commands, perceive surroundings, and make corresponding decisions [25]. However, these advancements are primarily limited to the visual domain [26–28]. While some research focuses on 3D visual grounding, these efforts are primarily aimed at RGB-D and LiDAR [29–33]. However, for autonomous driving and navigation, we argue that referring prompts cannot only emphasize positional relations, shapes, and categories, but target motion characteristics should be included, which is precisely the strength of radar. Radar is immune to adverse weather and can provide quantified distance, velocity, motion and azimuth while Radar Cross Section (RCS) and PCs provide qualitative semantic features, which enables great flexibility in describing objects, allowing for including both qualitative and quantitative characteristics. With the emergence of high-resolution 4D radar, this unexplored field is expected to be addressed. We aim to pioneer and release the potential of 4D radar for natural language-based multi-modal 3D target localization, precisely, individuals can locate specific objects with the format of 3D bounding box by describing features that 4D radar can perceive.

Based on these, we introduce 3D Referring Expression Comprehension (REC), also called as open-vocabulary 3D object detection [34], that locates specific objects based on textual descriptions, and establish the first radar-based 3D visual grounding dataset, Talk2Radar, and corresponding benchmark. Talk2Radar is built upon the well-known 4D radar dataset, View of Delft (VoD) [35], where each sample contains radar point clouds, LiDAR point clouds, an RGB image, and a textual reference prompt. Moreover, Talk2Radar contains the following two characteristics: **(i)** A prompt refers to one or more objects, and is more flexible and realistic. **(ii)** Text features contain target attributes perceivable by radar, while excluding any features perceivable by vision. Moreover, along with Talk2Radar, we propose a novel radar-text fusion model called T-RadarNet for 3D visual grounding. In T-RadarNet, **firstly**, we propose Deformable-FPN for the enhancement of irregular radar point cloud modeling; **secondly**, to efficiently fuse the features of radar and text, we devise a module called Gated Graph Fusion (GGF), building upon graph and gating mechanisms for neighborhood feature association and cross-modal feature matching. Notably, GGF can be transplanted to most PC detectors for 3D visual grounding with impressive



Fig. 1. Samples in Talk2Radar. The first and second row respectively presents referred objects in context of PC sensors (4D radar and LiDAR) and camera.

generalization. We summarize our contributions as follows:

- 1) This paper presents the first 4D radar-based 3D REC dataset, Talk2Radar, and its corresponding benchmark for subsequent studies.
- 2) A novel 3D REC model called T-RadarNet for radar-based 3D visual grounding, building upon devised Deformable-FPN and GGF, is proposed.
- 3) Comprehensive experiments are conducted to analyze and advance 4D radar-based visual grounding, thus also facilitate a holistic understanding in this field.

II. RELATED WORKS

A. 3D Referring Expression Comprehension in Traffic

As a challenging task based on multi-modal learning and 3D geometry, 3D REC aims to provide a textual prompt and locate one or more objects most closely matching it in the form of 3D bounding boxes. **(i) Datasets.** As Fig. 1 shows, [36] propose a 2D image-based REC dataset on driving scenarios upon Nuscenes [37], but providing LiDAR data of the same frame. [38] raises a monocular 3D grounding dataset upon KITTI [39]. [40] proposes a 3D grounding benchmark based on multi-camera and multi-frames for autonomous driving. **(ii) Methods.** [38] proposes a monocular-based 3D REC baseline model called Mono3DVG-TR. [41] raises a model for modeling complex 3D object relation called AFMNet. [31] propose a baseline model for LiDAR-based visual grounding upon Talk2Car dataset. Nevertheless, radar-based 3D REC is still unexplored and lacks full-scale analysis. Further, textual prompts of our Talk2Radar dataset contain more attributes of objects and context with qualitative or numerical description, and provide a realistic referring paradigm.

B. 3D Object Detection based on Point Cloud

3D object detection is vital for environmental perception for autonomous driving. Point cloud sensors mainly include LiDAR and 4D radar. LiDAR can provide rich geometric and depth features, while 4D radar can capture certain semantic features, motion, velocity, and depth features of objects. Currently, PC-based 3D detectors can be primarily divided into

Table I. Comparison of 3D visual grounding datasets in traffic

Datasets	Sensors	Objects	AvgExpr	Context
NuPro [40]	Camera	187,445	-	color size relation motion location
Talk2Car [36]	Camera	10,519	11.01	color size location relation
M3DRef [38]	Camera	8,228	53.24	size relation location color
Talk2Radar	4D radar, LiDAR	20,558	14.30	size motion location relation velocity depth

pillar-based and voxel-based. [42–44] are three fast pillar-based, which project point clouds onto a Bird’s-Eye View (BEV) and then extract features like image processing. [45–47] are three voxel-based detectors converting point clouds into voxel grids, which are known for simplicity, but they may suffer from low computation efficiency. Additionally, [48, 49] provide an anchor-free paradigm for 3D detection. [50] fuses different representations of point clouds dedicated to radar-based 3D detection. Based on the above, we fully consider two aspects in our T-RadarNet: **(i)** Extraction of irregular point cloud features, **(ii)** Dynamic weighting and separation of objects and clutter for high-quality fusion with text features.

III. TALK2RADAR DATASET

A. Data Collection and Annotation Process

Thanks to the renowned VoD dataset [35] in the field of radar perception, which is specifically designed for autonomous driving perception, equipped with the ZF FRGen21 4D mmWave radar, as well as a LiDAR and a stereo camera. We can engineer textual prompts upon finely annotated 3D bounding boxes of various road objects. Fig. 1 shows the samples while Fig. 2 presents the whole annotation process.

(1) Select Candidate Object(s). First, based on the developed Graphical User Interface (GUI) for annotation, we present the image with projected 3D bounding boxes for easy observation. Then, a specialist (annotator) with experience in the traffic clicks and selects the candidate boxes in the image that want to describe. The corresponding 3D bounding

Table II. Statistics of referent object number and point clouds in Talk2Radar

Objects	Pedestrian	Cyclist	Car	motor	truck	bicycle	rider	moped scooter	bicycle rack	human depiction	rider other	vehicle other
Sensor PC	3487 (17.0%)	3234 (15.8%)	9336 (45.6%)	73 (0.4%)	27 (0.1%)	2442 (11.9%)	159 (7.8%)	470 (2.3%)	1165 (5.7%)	48 (2.3%)	11 (-)	3 (-)
Radar1(1-frame)	2.0	3.8	3.6	3.4	17.7	1.4	1.7	1.8	3.0	-	2.5	-
Radar3(3-frame)	5.3	9.6	11.8	19.1	65.2	4.3	3.6	7.1	9.8	-	8.0	-
Radar5(5-frame)	7.4	12.1	18.7	44.4	128.0	7.0	4.2	9.6	14.3	-	9.5	-
LiDAR	258.9	211.5	771.6	1378.3	7338.4	174.2	273.9	232.9	215.5	-	6.0	-

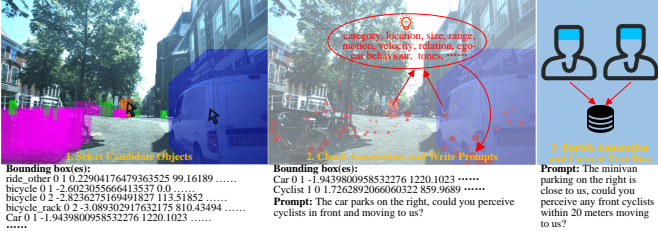


Fig. 2. Annotation process of Talk2Radar dataset.

box annotation will be saved. Here, the annotator prioritizes selecting objects within the radar’s Field of View (FoV).

(2) Check Annotations and Write Prompts. Based on chosen 3D bounding box(es), the annotator first check whether the bounding box(es) have errors on position or category. During annotation, we also attach compensated vector velocity and plane depth next to the corresponding PC for reference. Considering the detection error and object size, we generally describe the object depth as a range rather than a fixed value. For individual objects, annotators consider attributes such as category, spatial position relative to the ego vehicle, distance, velocity, motion trend, size, etc., but do not include color, and other information that radar cannot perceive. If multi-objects are selected, their spatial relationships are also considered.

(3) Enrich Annotation and Correct Text Bias. To avoid subjectivity and errors in text prompts, we implement a collaborative review and revision process involving two additional annotators after the initial annotation. This process serves to increase the diversity of descriptions to test the robustness and generalization of the model. Additionally, it allows for the discussion of subjective errors made by the initial annotator, followed by corrections upon reaching a consensus.

B. Dataset Statistics

We elucidate the quantitative statistics from the aspects of textual prompts and referent objects.

Textual Prompts. As Fig. 3 (a) presents, **firstly**, high-frequency words in the word cloud include both qualitative and quantitative descriptions, where rich mixed vocabulary benefits from the 4D radar’s multi-dimensional perception of objects, capturing quantitative features such as target velocity, motion direction, depth, etc., while also perceiving some degree of semantic features. This enables more detailed descriptions of specific objects and allows for fine-grained target clustering and filtering based on individual or partial target attributes. **Secondly**, as Fig. 3 (c) shows, the prompt length distribution

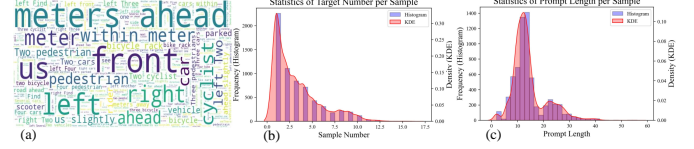


Fig. 3. Statistics of Talk2Radar dataset on referent objects and prompts.

in Talk2Radar is broad, whose average value is 14.30 (Table I, **AvgExpr**), allowing the model to learn a wide range of sentence patterns. This also increases the task difficulty, as the model must handle text prompts of varying patterns, structures, and lengths, correctly understand their hidden semantic representations, and query complex point cloud scenes.

Referent Objects. **Firstly**, as Table I presents, Talk2Radar contains 20,558 referent objects totally. **Secondly**, Table II shows the distribution of target quantities across 12 categories and the average PC quantity for each target category, including radar (1, 3 and 5 frames accumulated) and LiDAR. Car, Pedestrian and Cyclist are three primary referent categories in Talk2Radar. Evidently, although 4D radar has improved resolution, the gap in PC density compared to LiDAR still exists. **Thirdly**, as Fig. 3 (b) shows, in Talk2Radar, the referent object number of each sample range from 1 to 11, presenting a challenge for understanding complex scenes. Specifically, the model needs to adaptively filter out noise words in prompts and focus on the key characteristics of the referent object(s), while performing multiple Region-Of-Interest (ROI) queries in irregular point cloud contexts.

C. Metrics and Subset Settings

Metrics. We adopt Average Precision (AP) and Average Orientation Similarity (AOS), including 3D bounding box mAP and mAOS on the entire annotated and driving corridor area, consistent with VoD for comprehensive evaluation.

Subset Settings. We divide Talk2Radar into three subsets, sharing same IDs with VoD. The number of subsets for training, validation and test are 5139, 1296 and 2247, respectively. Since the test set annotation of VoD is not publicly available, models are evaluated on the validation set in this paper.

IV. METHODS

A. Overall Pipeline

Fig. 4 shows the detailed architecture of T-RadarNet. Given a frame of radar PC and a textual prompt as input, T-RadarNet will give the 3D grounding prediction of the specific object(s)

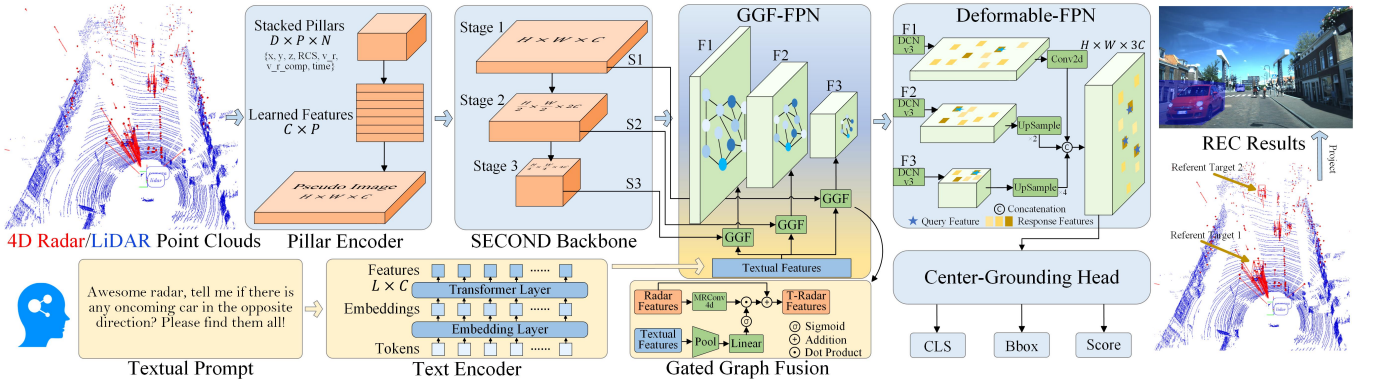


Fig. 4. The architecture of **T-RadarNet**. LiDAR is not the main modality, but it can also be used as the input of T-RadarNet.

upon the guidance of natural language. **Firstly**, for the primary PC feature extraction and modeling, considering efficient computation and scalability, we adopt the pillar encoder for 3D PC basic representation as a 2D pseudo image. Then, the concise SECOND backbone [46] is to extract three-stage radar PC features $\{F_R^{S1}, F_R^{S2}, F_R^{S3}\}$ with multi-scales. **Secondly**, we adopt transformers-based encoders (e.g. ALBERT) [51] for dynamic context representation of textual prompt. **Thirdly**, given the interference in radar PC context from multi-path clutter, aligning and fusing dense textual semantic features with sparse point clouds pose significant challenges. To address this, we design a graph-based strategy called Gated Graph Fusion (GGF), which associates ROI in the radar feature space and applies point-wise cross-modal gating between radar and text, yielding the most matched point cloud regions aligned with the text. Then, three-stage PC features and textual feature $F_T \in \mathbb{R}^{L \times C}$ are fed into GGF-FPN, which consists of GGF modules for cross-modal fusion and outputs three-scale text-conditional radar features $\{F_{R|T}^{S1}, F_{R|T}^{S2}, F_{R|T}^{S3}\}$. **Fourthly**, given the irregularity and sparsity of radar PC, conventional convolutions struggle to finely model them. Hence, we propose Deformable-FPN based on deformable convolutions [52], which provide high-quality PC features queried by the textual prompt to the grounding head for localization. **Lastly**, leveraging the efficiency of anchor-free detectors, we adopt the center-based detection head [48] and employ the deformable convolution-based separable localization head for text-referenced point cloud object localization.

B. Gated Graph Fusion

For one-stage deep radar PC feature $F_R \in \mathbb{R}^{H \times W \times C_r}$, we first construct a graph-based map $\mathcal{G} = G(F_R)$ to aggregate neighbour features and associate the potential object areas. We implement the graph convolution as Eq. (1) presents:

$$\begin{aligned} \hat{\mathcal{G}} &= H(\mathcal{G}, \mathcal{W}) \\ &= \text{Update}(\text{Aggregate}(\mathcal{G}, W_{agg}), W_{update}), \end{aligned} \quad (1)$$

where W_{agg} and W_{update} are two learnable weights for feature aggregation and update. Exactly, the aggregation operation calculates the representation of the current node by aggregating features of neighbouring nodes, which is presented in Eq. (2):

$$\hat{F}_R^i = h(F_R^i, g(F_R^i, \mathcal{N}(F_R^i), W_{agg}), W_{update}), \quad (2)$$

where $\mathcal{N}(F_R^i)$ is the set of neighbour nodes of F_R^i . Considering the efficiency of graph feature aggregation, we employ Max-Relative Graph Convolution [53], which is shown in Eq. (3) and (4) as below:

$$g(\cdot) = \hat{F}_R^i = \max(\{F_R^i - F_R^j \mid j \in \mathcal{N}(F_R^i)\}), \quad (3)$$

$$h(\cdot) = \hat{F}_R^i = \hat{F}_R^i W_{update}, \quad (4)$$

The above constructs the radar graph feature $F_{\mathcal{G}(R)} \in \mathbb{R}^{H \times W \times C_r}$ in one stage of three.

For the textual feature $F_T \in \mathbb{R}^{L \times C}$, we first adopt max-pooling along the token dimension to extract abstract high-level semantic information. Then, to align with the radar graph feature $F_{\mathcal{G}(R)}$, a linear transformation is exerted on it and we obtain the abstract textual feature $\hat{F}_T \in \mathbb{R}^{1 \times 1 \times C}$. Further, to effectively suppress radar noise points and focus on object ROI, we adopt a cross-modal gating strategy. Specifically, we obtain the weights of the linearly transformed textual features through Sigmoid activation and multiply them point-wise with the radar graph feature $F_{\mathcal{G}(R)}$. Finally, the feature is enhanced by addition with $F_{\mathcal{G}(R)}$ by a residual path. The process is shown in Eq. (5) and (6):

$$\hat{F}_T = \text{MaxPool}(F_T), \quad (5)$$

$$F_{R|T} = F_{\mathcal{G}(R)} \odot \sigma(\hat{F}_T \cdot W_T) + F_{\mathcal{G}(R)}, \quad (6)$$

where \odot and σ denote point-wise multiplication and Sigmoid.

C. Deformable FPN

To enhance representation of text-conditioned three-stage point cloud features $\{F_{R|T}^{S1}, F_{R|T}^{S2}, F_{R|T}^{S3}\}$, we first exert the efficient deformable convolutions [52] on three maps to perform adaptive sparse sampling and modeling of key features. For the current element r_0 in the one-stage radar map, the deformable convolution can be formulated as Eq. (7):

$$y(r_0) = \sum_{g=1}^G \sum_{k=1}^K w_g m_{gk} x_g(r_0 + r_k + \Delta r_{gk}), \quad (7)$$

Table III. Overall performances on Talk2Radar (**Best Radar**, **Best LiDAR**, Best Performance. **Car**, **Pedestrian** and **Cyclist** provide specialized mAPs.)

Models	Sensors	Text Encoder	Fusion	Entire Annotated Area (EAA)					Driving Corridor Area (DCA)				
				Car	Pedestrian	Cyclist	mAP	mAOS	Car	Pedestrian	Cyclist	mAP	mAOS
PointPillars (SFPN)	Radar5	ALBERT	HDP	18.92	9.79	12.47	13.73	12.91	39.20	10.25	14.93	21.46	20.19
SECOND (SFPN)	Radar5	ALBERT	HDP	17.70	7.67	10.58	11.98	11.06	38.17	8.62	14.95	20.58	19.77
CenterFormer	Radar5	ALBERT	HDP	17.26	6.79	9.27	11.11	10.79	19.56	9.13	12.03	13.57	13.02
CenterPoint (Pillar-SFPN)	Radar5	ALBERT	HDP	18.98	5.30	14.96	13.08	12.20	40.53	8.57	15.66	21.59	20.25
PointPillars (SFPN)	Radar5	ALBERT	MHCA	5.18	5.76	6.63	5.86	3.58	13.34	4.36	8.79	8.83	7.66
SECOND (SFPN)	Radar5	ALBERT	MHCA	4.98	3.69	4.24	4.30	2.24	10.67	3.50	7.03	7.07	6.57
CenterFormer	Radar5	ALBERT	MHCA	4.53	3.48	4.00	4.00	2.03	8.77	3.52	6.69	6.33	5.92
CenterPoint (Pillar-SFPN)	Radar5	ALBERT	MHCA	5.21	4.57	5.13	4.97	3.12	12.70	4.07	7.70	8.16	7.51
MSSG [31]	Radar5	GRU	-	12.53	5.08	8.47	8.69	7.03	18.93	7.88	9.40	12.07	11.67
AFMNet [41]	Radar5	GRU	-	11.98	6.87	9.16	9.34	7.72	18.62	8.21	10.06	12.30	11.79
T-RadarNet	Radar5	ALBERT	GGF	24.68	9.71	15.74	16.71	14.88	42.58	10.13	17.82	23.51	22.37
CenterPoint (Pillar-SFPN)	LiDAR	ALBERT	HDP	28.16	6.21	17.46	17.28	16.03	43.43	6.87	27.18	25.83	24.93
CenterPoint (Pillar-SFPN)	LiDAR	ALBERT	MHCA	6.56	5.04	5.33	5.64	4.86	13.60	4.52	7.32	8.48	7.89
MSSG [31]	LiDAR	GRU	-	15.38	7.52	11.67	11.52	9.76	23.27	8.68	13.51	15.15	14.75
AFMNet [41]	LiDAR	GRU	-	16.13	7.68	12.51	12.11	9.92	24.50	9.07	13.87	15.81	15.11
T-RadarNet	LiDAR	ALBERT	GGF	24.91	12.74	18.67	18.77	17.20	48.98	14.69	27.24	30.30	29.89

where G and K denote element aggregation groups and the feature dimension. w_g is the projection weights of the group. m_{gk} is the modulation scalar of the k -th sampling point while Δr_{gk} is the offset of sampling position r_k in the g -th group.

Then $F_{R|T}^{S_2} \in \mathbb{R}^{\frac{H}{2} \times \frac{W}{2} \times 2C}$ and $F_{R|T}^{S_3} \in \mathbb{R}^{\frac{H}{4} \times \frac{W}{4} \times 4C}$ are upsampled to the same size as $F_{R|T}^{S_1}$ by transposed convolution. Finally, three-scale feature maps are concatenated to obtain high-resolution aggregated point cloud features $F_{Agg} \in \mathbb{R}^{H \times W \times 3C}$ with multi-receptive fields.

D. Training Objectives

The center-based detection head first produces class-wise heatmaps to predict the center location of the detected objects for each class. Afterward, the following properties of each object are supervised following CenterPoint [48]: the sub-voxel location refinement, the height-above-ground, the 3D size, and the orientation angle. The proposed T-RadarNet is trained with the following loss:

$$\mathcal{L}_{\text{total}} = \mathcal{L}_{\text{hm}} + \beta \sum_{r \in \mathbf{BB}} \mathcal{L}_{\text{smooth-l}_1}(\widehat{\Delta r^a}, \Delta r^a), \quad (8)$$

where \mathcal{L}_{hm} is the classification loss that supervises the heatmap quality of the center-based detection head using a focal loss [54], and $\mathbf{BB} = \{x, y, z, l, h, w, \theta\}$ which indicates the smooth-L1 loss supervises the regression of the box center (for slight modification based on heatmap peak guidance), dimensions, and orientation. β is the weight to balance the two components of the loss, which is set to 0.25 by default.

V. EXPERIMENTS

A. Implementation Settings

Model Settings. **Firstly**, for our T-RadarNet, we set the token length as 30 upon ALBERT [55]. N in the pillar encoder is set as 10 and 32 for radar and LiDAR, respectively while C

is 64. We select PC-based detectors with various paradigms for comparison and analysis, including PointPillars (pillar-based) [42], CenterPoint (anchor-free) [48], SECOND (voxel-based) [46] and CenterFormer (transformer-based) [49]. Further, we also include dedicated 3D PC grounding model MSSG [31] and AFMNet [41]. **Secondly**, fusion methods including inductive bias-based HDP [56], attention-based MHCA [28] and our GGF. **Thirdly**, SECONDFPN [46], ASPP [43] and CSP-FPN [57] are included for comparison with Deformable FPN.

Dataset Settings. We mainly focus on objects of three primary categories, *i.e.*, Car, Cyclist, and Pedestrian, in Talk2Radar while we also train and test models on all categories (in supplementary materials). We train and test models on both 4D radar and LiDAR data. Further, to validate the generalization of our T-RadarNet, we also train and test it on Talk2Car [36], where it provides LiDAR PC and each sample contains one textual prompt for a unique object.

Training and Evaluation Settings. For Talk2Radar, all models are trained on four RTX A4000 with a batch size of 4 for 80 epochs. The initial learning rate is set 1e-3 with a cosine scheduler. We choose AdamW for optimization with a weight decay of 5e-4. For Talk2Car, we set the initial learning rate as 1e-2 while other settings are kept the same with Talk2Radar.

B. Quantitative Results

Overall Performances. As Table III shows, on the whole, T-RadarNet outperforms other models in most aspects whatever on 4D radar or LiDAR. For other models, we find that models based on pillar encoding perform better than those based on voxels, and models based on self-attention do not significantly outperform those based on convolution. Regarding fusion, models using MHCA perform worse than those using gating and dot-product operations. This phenomenon is particularly evident with five-frame radar data (Radar5).

Performances on Various Prompts. As Table IV shows, when we compare the performance of T-RadarNet on prompts

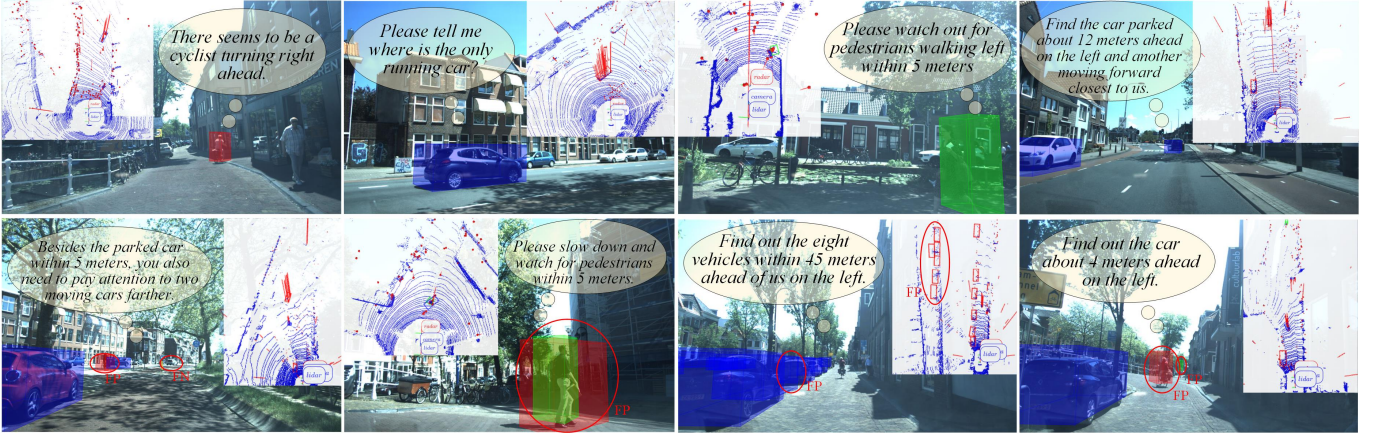


Fig. 5. Prediction by T-RadarNet. The first row presents correct cases while the second shows problematic cases (FN: False Negative, FP: False Positive).

Table IV. Comparison (mAP) of radar and LiDAR upon various prompts for T-RadarNet

Prompt	Motion			Depth			Velocity		
Sensors	Car	Pedes	Cyclist	Car	Pedes	Cyclist	Car	Pedes	Cyclist
Radar1	26.10	5.33	11.07	32.68	12.69	24.72	26.92	13.99	18.45
Radar3	35.92	11.05	15.43	40.68	18.66	31.69	33.78	20.51	25.78
Radar5	36.72	11.54	16.27	42.50	19.63	32.03	35.50	20.79	25.73
LiDAR	33.56	8.80	13.58	45.68	20.54	38.60	12.63	7.63	8.24

Table V. Statistics of predicted objects mAP by depth upon 5-frame radar

Objects	0-10 (m)	10-20	20-30	30-40	40-50	50+
Car	42.57	44.57	23.26	18.36	10.04	1.32
Pedestrian	15.54	7.17	3.14	2.06	4.54	0.0
Cyclist	29.15	11.39	14.14	3.94	1.78	0.0

with queries of types on motion, depth and velocity, the radar-based model outperforms LiDAR-based on prompts regarding motion and velocity, which is more obvious on velocity-based prompts. Besides, as LiDAR can reason the object motion upon PC object appearances, the gap between radar and LiDAR on motion query is not large. For the depth-related prompts, LiDAR obtains the advantage to some extent.

Precision by Piece-wise Depths. Table V presents the mAP of predicted objects by segmented depths upon 5-frame radar. Small-object grounding is doubtless a challenge.

Generalization Performances. To validate the generalization of T-RadarNet, we train and test on Talk2Car, which is a REC benchmark providing LiDAR data for object grounding. As Table VII shows, our T-RadarNet outperforms the baseline and the other two models, which proves the effectiveness and generalization of T-RadarNet for PC-based 3D REC.

C. Ablation Experiments

Table VI presents the ablation results of T-RadarNet.

GGF. When we replace the MRConv4D (GConv) with normal convolution, mAP drops remarkably, which is the same circumstance with pooling for textual semantics abstraction.

Necks. Our Deformable FPN outperforms other necks overall, indicating the preminent modeling of point clouds.

Table VI. Ablation comparison of T-RadarNet upon 5-Frame radar data

Methods	EAA			DCA		
	Car	Ped	Cyc	Car	Ped	Cyc
Gated Graph Fusion						
GConv → Conv	20.03	7.56	13.70	36.56	7.99	13.58
MaxPool → AvgPool	21.40	8.04	13.88	38.67	7.87	13.78
GConv + MaxPool	24.68	9.71	15.74	42.58	10.13	17.82
Necks (Feature Pyramid Networks)						
ASPP	23.01	9.56	14.59	38.06	9.27	16.60
SFPN	23.57	9.26	14.03	41.56	9.02	16.42
CSP-FPN	23.53	9.70	14.38	41.58	9.31	17.03
DeformableFPN	24.68	9.71	15.74	42.58	10.13	17.82
Fusion Methods						
HDP	20.07	6.52	14.86	39.53	8.62	15.85
MHCA	7.79	5.02	5.36	13.69	5.81	9.35
GGF	24.68	9.71	15.74	42.58	10.13	17.82
Fusion Locations						
neck-head	17.53	8.10	12.06	38.56	5.03	14.59
backbone-neck	24.68	9.71	15.74	42.58	10.13	17.82

Table VII. Performances on Talk2Car benchmark for Lidar-based 3D REC, where AP_A and AP_B follow MSSG [31] that define different IoU thresholds for each category.

Models	BEV AP		3D AP	
	AP_A	AP_B	AP_A	AP_B
Talk2Car [36]	30.6	24.4	27.9	19.1
MSSG [31]	27.8	26.1	31.9	20.3
AFMNet [41]	45.3	33.1	41.9	20.7
T-RadarNet	52.8	39.9	47.2	30.5

Fusion Methods. Our proposed GGF presents a better result than other fusion methods, implying a more efficient approach to aligning and embedding textual semantics to point clouds. Although MHCA can model global cross-modal similarity, its performance is sub-optimal when dealing with irregular point clouds containing both targets and ghosting in radar data.

Fusion Locations. Previous works [41, 58–61] prove the effectiveness of PC-text fusion on the location of models,

including neck-to-head and backbone-to-neck. In Talk2Radar, we find that when fusing two modalities on the output of the backbone is better than after the neck.

D. Visualization and Discussion

Fig. 5 presents the prediction results by T-RadarNet based on the 5-frame accumulated radar PC, including visualization on the image plane and BEV view in the PC context. For the correct prediction results in the first row, we can see our T-RadarNet possesses the capacity to understand the textual prompts with different lengths and localize the correct objects among complex point cloud contexts, including single and multiple referent objects. However, there are still some problems with this task, in the second row, we can see the serious false positive cases in the prediction bounding boxes, implying that efficient modeling of radar PC features and adaptive filtering of non-object clutter are still a challenge.

VI. CONCLUSION

This paper proposes a novel task: 4D mmWave radar-based 3D referring expression comprehension (visual grounding), aimed at embodied intelligence and interactive perception with full weather operational, low-cost sensor. The first dataset on such task, Talk2Radar, has been presented by fully exploiting object detection characteristics of 4D mmWave radar. Talk2Radar includes abundant textual prompts and object distributions, as well as LiDAR. Through extensive experiments, the corresponding benchmark has been provided by proposing an efficient radar-based 3D REC model, T-RadarNet. In T-RadarNet, we design an effective module, Gated Graph Fusion, for the alignment and fusion of textual and 4D radar point cloud features. Additionally, Deformable FPN is proposed to adequately model irregular and sparse point cloud features. Having all the aforementioned contributions, we aim to advance the interactive perception capabilities of 4D radar for environmental understanding in autonomous driving.

REFERENCES

- [1] Shanliang Yao, Runwei Guan, Xiaoyu Huang, Zhuoxiao Li, Xiangyu Sha, Yong Yue, Eng Gee Lim, Hyungjoon Seo, Ka Lok Man, Xiaohui Zhu, et al., "Radar-camera fusion for object detection and semantic segmentation in autonomous driving: A comprehensive review," *IEEE Transactions on Intelligent Vehicles*, vol. 9, no. 1, pp. 2094–2128, 2024.
- [2] Shanliang Yao, Runwei Guan, Zitian Peng, Chenhang Xu, Yilu Shi, Yong Yue, Eng Gee Lim, Hyungjoon Seo, Ka Lok Man, Xiaohui Zhu, et al., "Radar perception in autonomous driving: Exploring different data representations," *arXiv:2312.04861*, 2023.
- [3] Jianan Liu, Weiye Xiong, Liping Bai, Yuxuan Xia, Tao Huang, Wanli Ouyang, and Bing Zhu, "Deep instance segmentation with automotive radar detection points," *IEEE Transactions on Intelligent Vehicles*, vol. 8, no. 1, pp. 84–94, 2023.
- [4] Matthias Zeller, Vardeep S Sandhu, Benedikt Mersch, Jens Behley, Michael Heidingsfeld, and Cyrill Stachniss, "Radar velocity transformer: Single-scan moving object segmentation in noisy radar point clouds," in *IEEE International Conference on Robotics and Automation (ICRA)*. IEEE, 2023, pp. 7054–7061.
- [5] Alexander Popov, Patrik Gebhardt, Ke Chen, and Ryan Oldja, "Nvradar-net: Real-time radar obstacle and free space detection for autonomous driving," in *IEEE International Conference on Robotics and Automation (ICRA)*. IEEE, 2023, pp. 6958–6964.
- [6] Yanlong Yang, Jianan Liu, Tao Huang, Qing-Long Han, Gang Ma, and Bing Zhu, "RaLiBEV: Radar and LiDAR BEV fusion learning for anchor box free object detection systems," 2022, *arXiv:2211.06108*.
- [7] Jisong Kim, Minjae Seong, Geonho Bang, Dongsuk Kum, and Jun Won Choi, "Rcm-fusion: Radar-camera multi-level fusion for 3d object detection," in *Proceedings of the IEEE International Conference on Robotics and Automation (ICRA)*, 2024.
- [8] Youngseok Kim, Juyeb Shin, Sanmin Kim, In-Jae Lee, Jun Won Choi, and Dongsuk Kum, "Crn: Camera radar net for accurate, robust, efficient 3d perception," in *Proceedings of the IEEE/CVF International Conference on Computer Vision*, 2023, pp. 17615–17626.
- [9] Ziyang Hong, Yvan Petillot, and Sen Wang, "Radarslam: Radar based large-scale slam in all weathers," in *2020 IEEE/RSJ International Conference on Intelligent Robots and Systems (IROS)*, 2020, pp. 5164–5170.
- [10] Yeong Sang Park, Young-Sik Shin, Joowan Kim, and Ayoung Kim, "3d ego-motion estimation using low-cost mmwave radars via radar velocity factor for pose-graph slam," *IEEE Robotics and Automation Letters*, vol. 6, no. 4, pp. 7691–7698, 2021.
- [11] Tao Huang, Jianan Liu, Xi Zhou, Dinh C Nguyen, Mostafa Rahimi Azghadi, Yuxuan Xia, Qing-Long Han, and Sumei Sun, "V2X co-operative perception for autonomous driving: Recent advances and challenges," 2023, *arXiv:2310.03525*.
- [12] Zeyu Han, Jiahao Wang, Zikun Xu, Shuocheng Yang, Lei He, Shaobing Xu, and Jianqiang Wang, "4d millimeter-wave radar in autonomous driving: A survey," *arXiv preprint arXiv:2306.04242*, 2023.
- [13] Lili Fan, Junhao Wang, Yuanmeng Chang, Yuke Li, Yutong Wang, and Dongpu Cao, "4d mmwave radar for autonomous driving perception: A comprehensive survey," *IEEE Transactions on Intelligent Vehicles*, pp. 1–15, 2024, doi: 10.1109/TIV.2024.3380244.
- [14] Lianqing Zheng, Sen Li, Bin Tan, Long Yang, Sihan Chen, Libo Huang, Jie Bai, Xichan Zhu, and Zhixiong Ma, "Refusion: Fusing 4-d radar and camera with bird's-eye view features for 3-d object detection," *IEEE Transactions on Instrumentation and Measurement*, vol. 72, pp. 1–14, 2023.
- [15] Weiye Xiong, Jianan Liu, Tao Huang, Qing-Long Han, Yuxuan Xia, and Bing Zhu, "LXL: LiDAR excluded lean 3D object detection with 4D imaging radar and camera fusion," *IEEE Transactions on Intelligent Vehicles*, vol. 9, no. 1, pp. 79–92, October 2024.
- [16] Jun Zhang, Huayang Zhuge, Zhenyu Wu, Guohao Peng, Mingxing Wen, Yiyao Liu, and Danwei Wang, "4dradarslam: A 4d imaging radar slam system for large-scale environments based on pose graph optimization," in *2023 IEEE International Conference on Robotics and Automation (ICRA)*, 2023, pp. 8333–8340.
- [17] Jianan Liu, Guanhua Ding, Jinping Xia, Yuxuan Sun, Tao Huang, Lihua Xie, and Bing Zhu, "Which framework is suitable for online 3D multi-object tracking for autonomous driving with automotive 4D imaging radar?," in *Proceedings of the IEEE 35th Intelligent Vehicles Symposium (IV)*, 2024, *arXiv:2309.06036*.
- [18] Zhiwei Lin, Zhe Liu, Zhongyu Xia, Xinhao Wang, Yongtao Wang, Shengxiang Qi, Yang Dong, Nan Dong, Le Zhang, and Ce Zhu, "Rcbvdt: Radar-camera fusion in bird's eye view for 3d object detection," in *Proceedings of the IEEE/CVF Conference on Computer Vision and Pattern Recognition (CVPR)*, 2024.
- [19] Felix Fent, Andras Palffy, and Holger Caesar, "Dpft: Dual perspective fusion transformer for camera-radar-based object detection," *arXiv:2404.03015*, 2024.
- [20] Runwei Guan, Shanliang Yao, Xiaohui Zhu, Ka Lok Man, Eng Gee Lim, Jeremy Smith, Yong Yue, and Yutao Yue, "Achelous: A fast unified water-surface panoptic perception framework based on fusion of monocular camera and 4d mmwave radar," in *2023 IEEE 26th International Conference on Intelligent Transportation Systems (ITSC)*. IEEE, 2023, pp. 182–188.
- [21] Runwei Guan, Shanliang Yao, Lulu Liu, Xiaohui Zhu, Ka Lok Man, Yong Yue, Jeremy Smith, Eng Gee Lim, and Yutao Yue, "Mask-vrdet: A robust riverway panoptic perception model based on dual graph fusion of vision and 4d mmwave radar," *Robotics and Autonomous Systems*, vol. 171, pp. 104572, 2024.
- [22] Runwei Guan, Liye Jia, Fengyufan Yang, Shanliang Yao, Erick Purwanto, Xiaohui Zhu, Eng Gee Lim, Jeremy Smith, Ka Lok Man, and Yutao Yue, "Watervg: Waterway visual grounding based on text-guided vision and mmwave radar," *arXiv:2403.12686*, 2024.
- [23] Tsun-Hsuan Wang, Alaa Maalouf, Wei Xiao, Yutong Ban, Alexander Amini, Guy Rosman, Sertac Karaman, and Daniela Rus, "Drive anywhere: Generalizable end-to-end autonomous driving with multi-modal foundation models," *arXiv:2310.17642*, 2023.
- [24] Can Cui, Yunsheng Ma, Xu Cao, Wenqian Ye, Yang Zhou, Kaizhao

- Liang, Jintai Chen, Juanwu Lu, Zichong Yang, Kuei-Da Liao, et al., “A survey on multimodal large language models for autonomous driving,” in *Proceedings of the IEEE/CVF Winter Conference on Applications of Computer Vision*, 2024, pp. 958–979.
- [25] Junlin Xie, Zhihong Chen, Ruifei Zhang, Xiang Wan, and Guanbin Li, “Large multimodal agents: A survey,” *arXiv:2402.15116*, 2024.
- [26] Chonghao Sima, Katrin Renz, Kashyap Chitta, Li Chen, Hanxue Zhang, Chengen Xie, Ping Luo, Andreas Geiger, and Hongyang Li, “Drivelm: Driving with graph visual question answering,” *arXiv:2312.14150*, 2023.
- [27] Chang Liu, Henghui Ding, and Xudong Jiang, “Gres: Generalized referring expression segmentation,” in *Proceedings of the IEEE/CVF conference on computer vision and pattern recognition*, 2023, pp. 23592–23601.
- [28] Dongming Wu, Wencheng Han, Tiancai Wang, Xingping Dong, Xiangyu Zhang, and Jianbing Shen, “Referring multi-object tracking,” in *Proceedings of the IEEE/CVF conference on computer vision and pattern recognition*, 2023, pp. 14633–14642.
- [29] Panos Achlioptas, Ahmed Abdelreheem, Fei Xia, Mohamed Elhoseiny, and Leonidas Guibas, “Referit3d: Neural listeners for fine-grained 3d object identification in real-world scenes,” in *Proceedings of the 16th European Conference on Computer Vision*, 2020, pp. 422–440.
- [30] Lichen Zhao, Daigang Cai, Lu Sheng, and Dong Xu, “3dvg-transformer: Relation modeling for visual grounding on point clouds,” in *Proceedings of the IEEE/CVF International Conference on Computer Vision*, 2021, pp. 2928–2937.
- [31] Wenhao Cheng, Junbo Yin, Wei Li, Ruigang Yang, and Jianbing Shen, “Language-guided 3d object detection in point cloud for autonomous driving,” *arXiv:2305.15765*, 2023.
- [32] Senqiao Yang, Jiaming Liu, Ray Zhang, Mingjie Pan, Zoey Guo, Xiaoqi Li, Zehui Chen, Peng Gao, Yandong Guo, and Shanghang Zhang, “Lidar-llm: Exploring the potential of large language models for 3d lidar understanding,” *arXiv:2312.14074*, 2023.
- [33] Georg Hess, Adam Tonderski, Christoffer Petersson, Kalle Åström, and Lennart Svensson, “Lidarcip or: How i learned to talk to point clouds,” in *Proceedings of the IEEE/CVF Winter Conference on Applications of Computer Vision*, 2024, pp. 7438–7447.
- [34] Xingcheng Zhou, Mingyu Liu, Ekim Yurtsever, Bare Luka Zagar, Walter Zimmer, Hu Cao, and Alois C. Knoll, “Vision language models in autonomous driving: A survey and outlook,” *IEEE Transactions on Intelligent Vehicles*, 2024, doi:10.1109/TIV.2024.3402136.
- [35] Andras Palffy, Ewoud Pool, Sriramannarayana Baratam, Julian FP Kooij, and Dariu M Gavrilă, “Multi-class road user detection with 3+ 1d radar in the view-of-delft dataset,” *IEEE Robotics and Automation Letters*, vol. 7, no. 2, pp. 4961–4968, 2022.
- [36] Thierry Deruyttere, Simon Vandenhennde, Dusan Grujicic, Luc Van Gool, and Marie Francine Moens, “Talk2car: Taking control of your self-driving car,” in *Proceedings of the 2019 Conference on Empirical Methods in Natural Language Processing and the 9th International Joint Conference on Natural Language Processing (EMNLP-IJCNLP)*, 2019, pp. 2088–2098.
- [37] Holger Caesar, Varun Bankiti, Alex H Lang, Sourabh Vora, Venice Erin Liong, Qiang Xu, Anush Krishnan, Yu Pan, Giancarlo Baldan, and Oscar Beijbom, “nuscenes: A multimodal dataset for autonomous driving,” in *Proceedings of the IEEE/CVF Conference on Computer Vision and Pattern Recognition*, 2020, pp. 11621–11631.
- [38] Yang Zhan, Yuan Yuan, and Zhitong Xiong, “Mono3dvg: 3d visual grounding in monocular images,” in *Proceedings of the AAAI Conference on Artificial Intelligence*, 2024, vol. 38, pp. 6988–6996.
- [39] Andreas Geiger, Philip Lenz, and Raquel Urtasun, “Are we ready for autonomous driving? the kitti vision benchmark suite,” in *2012 IEEE conference on computer vision and pattern recognition*. IEEE, 2012, pp. 3354–3361.
- [40] Dongming Wu, Wencheng Han, Tiancai Wang, Yingfei Liu, Xiangyu Zhang, and Jianbing Shen, “Language prompt for autonomous driving,” *arXiv preprint arXiv:2309.04379*, 2023.
- [41] Ali Solgi and Mehdi Ezoji, “A transformer-based framework for visual grounding on 3d point clouds,” in *2024 20th CSI International Symposium on Artificial Intelligence and Signal Processing (AISP)*. IEEE, 2024, pp. 1–5.
- [42] Alex H Lang, Sourabh Vora, Holger Caesar, Lubing Zhou, Jiong Yang, and Oscar Beijbom, “Pointpillars: Fast encoders for object detection from point clouds,” in *Proceedings of the IEEE/CVF conference on computer vision and pattern recognition*, 2019, pp. 12697–12705.
- [43] Jinyu Li, Chenxu Luo, and Xiaodong Yang, “Pillarnext: Rethinking network designs for 3d object detection in lidar point clouds,” in *Proceedings of the IEEE/CVF Conference on Computer Vision and Pattern Recognition*, 2023, pp. 17567–17576.
- [44] Weixin Mao, Tiancai Wang, Diankun Zhang, Junjie Yan, and Osamu Yoshie, “Pillarnet: Embracing backbone scaling and pretraining for pillar-based 3d object detection,” *IEEE Transactions on Intelligent Vehicles*, 2024.
- [45] Yin Zhou and Oncel Tuzel, “Voxelnet: End-to-end learning for point cloud based 3d object detection,” in *Proceedings of the IEEE conference on computer vision and pattern recognition*, 2018, pp. 4490–4499.
- [46] Yan Yan, Yuxing Mao, and Bo Li, “Second: Sparsely embedded convolutional detection,” *Sensors*, vol. 18, no. 10, pp. 3337, 2018.
- [47] Yukang Chen, Jianhui Liu, Xiangyu Zhang, Xiaojuan Qi, and Jiaya Jia, “Voxelnext: Fully sparse voxelnet for 3d object detection and tracking,” in *Proceedings of the IEEE/CVF Conference on Computer Vision and Pattern Recognition*, 2023, pp. 21674–21683.
- [48] Tianwei Yin, Xingyi Zhou, and Philipp Krahenbuhl, “Center-based 3d object detection and tracking,” in *Proceedings of the IEEE/CVF conference on computer vision and pattern recognition*, 2021, pp. 11784–11793.
- [49] Zixiang Zhou, Xiangchen Zhao, Yu Wang, Panqu Wang, and Hassan Foroosh, “Centerformer: Center-based transformer for 3d object detection,” in *European Conference on Computer Vision*. Springer, 2022, pp. 496–513.
- [50] Jianan Liu, Qiuchi Zhao, Weiye Xiong, Tao Huang, Qing-Long Han, and Bing Zhu, “SMURF: Spatial multi-representation fusion for 3d object detection with 4d imaging radar,” *IEEE Transactions on Intelligent Vehicles*, vol. 9, no. 1, pp. 799–812, 2023.
- [51] Thomas Wolf, Lysandre Debut, Victor Sanh, Julien Chaumond, Clement Delangue, Anthony Moi, Pierric Cistac, Tim Rault, Rémi Louf, Morgan Funtowicz, et al., “Huggingface’s transformers: State-of-the-art natural language processing,” *arXiv preprint arXiv:1910.03771*, 2019.
- [52] Wenhao Wang, Jifeng Dai, Zhe Chen, Zhenhang Huang, Zhiqi Li, Xizhou Zhu, Xiaowei Hu, Tong Lu, Lewei Lu, Hongsheng Li, et al., “Internimage: Exploring large-scale vision foundation models with deformable convolutions,” in *Proceedings of the IEEE/CVF Conference on Computer Vision and Pattern Recognition*, 2023, pp. 14408–14419.
- [53] Guohao Li, Matthias Muller, Ali Thabet, and Bernard Ghanem, “Deepgcns: Can gcns go as deep as cnns?,” in *Proceedings of the IEEE/CVF international conference on computer vision*, 2019, pp. 9267–9276.
- [54] Tsung-Yi Lin, Priya Goyal, Ross Girshick, Kaiming He, and Piotr Dollar, “Focal loss for dense object detection,” in *Proceedings of the IEEE International Conference on Computer Vision (ICCV)*, Oct 2017.
- [55] Zhenzhong Lan, Mingda Chen, Sebastian Goodman, Kevin Gimpel, Piyush Sharma, and Radu Soricut, “Albert: A lite bert for self-supervised learning of language representations,” 2020.
- [56] Chaoyang Zhu, Yiyi Zhou, Yunhang Shen, Gen Luo, Xingjia Pan, Mingbao Lin, Chao Chen, Liujuan Cao, Xiaoshuai Sun, and Rongrong Ji, “Seqtr: A simple yet universal network for visual grounding,” in *European Conference on Computer Vision*. Springer, 2022, pp. 598–615.
- [57] Zheng Ge, Songtao Liu, Feng Wang, Zeming Li, and Jian Sun, “Yolox: Exceeding yolo series in 2021,” *arXiv preprint arXiv:2107.08430*, 2021.
- [58] Junha Roh, Karthik Desingh, Ali Farhadi, and Dieter Fox, “Language-refer: Spatial-language model for 3d visual grounding,” in *Conference on Robot Learning*. PMLR, 2022, pp. 1046–1056.
- [59] Shijia Huang, Yilun Chen, Jiaya Jia, and Liwei Wang, “Multi-view transformer for 3d visual grounding,” in *Proceedings of the IEEE/CVF Conference on Computer Vision and Pattern Recognition*, 2022, pp. 15524–15533.
- [60] Zoey Guo, Yiwen Tang, Ray Zhang, Dong Wang, Zhigang Wang, Bin Zhao, and Xuelong Li, “Viewrefer: Grasp the multi-view knowledge for 3d visual grounding,” in *Proceedings of the IEEE/CVF International Conference on Computer Vision*, 2023, pp. 15372–15383.
- [61] Shizhe Chen, Pierre-Louis Guhur, Makarand Tapaswi, Cordelia Schmid, and Ivan Laptev, “Language conditioned spatial relation reasoning for 3d object grounding,” *Advances in neural information processing systems*, vol. 35, pp. 20522–20535, 2022.